Graph analysis of resting state EEG functional networks in migraine

Master of Science Thesis

A.E. Smid

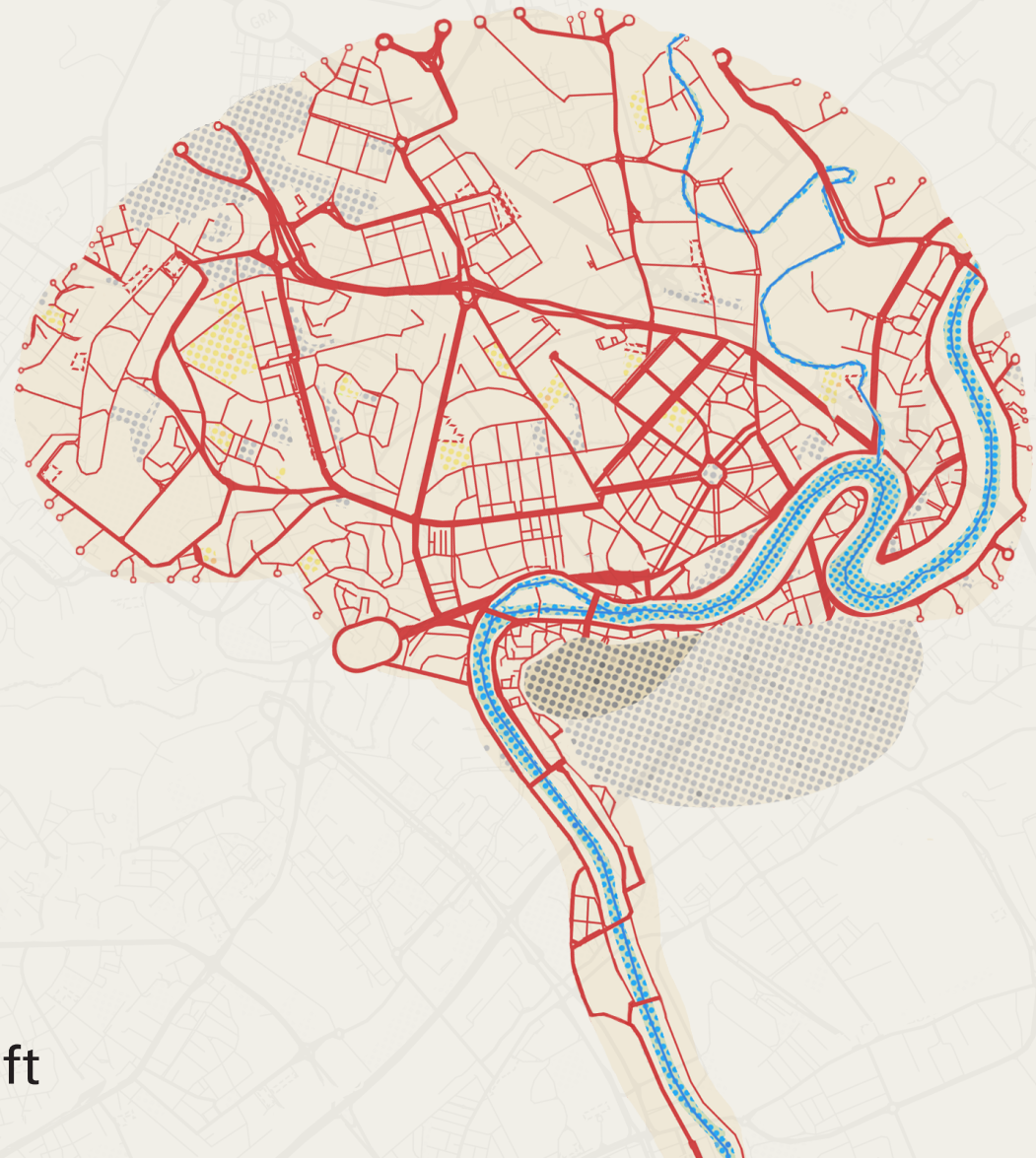

TU Delft

Graph analysis of resting state EEG functional networks in migraine

Master of Science Thesis

by

A.E. Smid

to obtain the degree of Master of Science in
Mechanical Engineering at Delft University of Technology,
to be defended publicly on Thursday April 19, 2018 at 03:00 PM.

Thesis committee:	dr. ir. A.C. Schouten,	TU Delft, chair
	Ir. M. J. L. Perenboom,	TU Delft, supervisor
	Drs. C. Wehrmann,	TU Delft
	Ir. M. L. van de Ruit,	TU Delft

An electronic version of this thesis is available at `http://repository.tudelft.nl/`.

TU Delft Delft University of Technology

Thanks!

Many thanks to my supervisor Thijs Perenboom, who taught me so much during this project. If there would be a best-daily-supervisor-award, I would definitely nominate him. Also, many thanks to Alfred Schouten, who guided me through the project.

Thanks to my family and friends, who've always supported me one way or another.

Many thanks to Tjerk for patiently listening during the course of this project. Lastly, special thanks to Lola, the illustrator queen.

Preface

All roads lead to Rome. This famous saying originates from the time of the Roman Empire, when the Romans were one of the first to construct a network of roads. The network facilitated fast and easy transport for the Roman army, to suppress any riot or revolution anywhere in the Empire. The title page of this thesis report comprises -literally- another Roman network, in the shape of a brain. The small island in the river is called *Isola Tiberina* and based on that island is the *Ospedale San Giovanni Calibita Fatebenefratelli*, where I spent three months in the crypts doing research on EEG analyses and functional connectivity.

Similar to the network of roads, the neuronal network in the brain is thought to be constructed in such a way that it facilitates fast and easy information transport. This thesis is about possible disruptions in the traffic of the network in the migraine brain.

There are many things we do not yet understand about migraine. For example, as a migraineur myself, I suffered way more migraine attacks in Rome than I do in the Netherlands, which possibly has to do with the weather. I am very happy to have contributed in research on migraine pathophysiology. P.J. Goadsby excellently described the importance of migraine research:

The key to the clinical approach to migraine is to understand its biology; this drives diagnosis and management, while allowing the clinician to provide a useful explanation to patients who seek information or diseasecontrol, or both. - **P.J. Goadsby**

With this in mind, I will extend this migraine research from neuronal networks to the field of social networks. For now, I hope you enjoy reading this thesis report.

Annemijn Smid
Delft, April 2018

Graph analysis of resting state EEG functional networks in migraine

Annemijn E. Smid

Department of Biomedical Engineering, Faculty of Mechanical, Maritime and Materials Engineering. Delft University of Technology.

***Abstract* - Migraine is associated with brain dysfunction, possibly due to disturbances in the interactions between distributed cortical regions. Detection of these disturbances in the topological organization of the brain's *functional network* would contribute to further understanding of migraine pathophysiology. Altered cortical responses to external stimulation of different modalities are observed in migraine patients, also between attacks (in the *interictal* state). However, it is yet unclear if abnormalities are detectable in the functional network at rest, i.e. without external stimulation. Here, we assessed abnormalities in migraine functional networks on a global and a local level, based on resting state electroencephalography (EEG) data and graph analysis. Scalp-wide (128-channel) eyes closed EEG was recorded in 18 episodic migraine patients with and without aura and 15 healthy controls. We calculated functional connectivity based on coherence and phase-lag index, and performed graph analysis to characterize network topology. The minimum spanning tree, a subgraph with maximum functional connectivity, was used for comparison. No significant differences were found in network topology, nor in functional connectivity strength between groups. These results demonstrate that this type of graph analyses are not sensitive to any possible abnormalities in the interictal migraine functional network in resting state. Brain dysfunction in migraine might occur only on a local level, making EEG-based graph analysis a less suitable technique to uncover such abnormalities.**

1. INTRODUCTION

Migraine is a highly disabling brain disorder and affects approximately 15% of the global population (Global Burden of Disease Survey, 2010). Migraine attacks consist of severe, pulsating headache, typically accompanied by nausea and/or sensitivity to light, sound or smell. One-third of migraineurs experience neurological symptoms (usually visual) preceding the headache phase, known as *aura* (Goadsby, 2003). The recurrent nature of migraine suggests an underlying abnormality in the functioning of the brain. However, it is yet unknown what mechanisms lead to the pathogenesis of attacks (Moulton et al., 2011; Scheffer et al., 2013; Hougaard et al., 2015). A better understanding of these mechanisms is necessary to improve our understanding of migraine pathophysiology and thereby improve treatment.

Previous research found that migraine is associated with altered processing of sensory information when evoked by an external stimulation (e.g., visual or magnetic). Such abnormalities in information processing have been reported even between attacks, in the *interictal state*. This might be due to an extreme responsiveness of cortical neurons, or neuronal *hyperexcitability* (Aurora and Wilkinson, 2007; Moulton et al., 2011). However, it is yet unclear if abnormalities are detectable without external stimulation, i.e. in the *resting state*.

Resting state studies focus on the characterization of patterns of simultaneously active brain regions (Allen et al., 2012). The brain can be understood as a structurally and functionally integrated network: the structural network corresponds to anatomical connections between neurons, but electrical pulses of neuronal communication comprise the *functional network* (Bullmore and Sporns, 2009). The functional network might not always coincide with the underlying infrastructure of the structural network (Rubinov and Sporns, 2009). As an analogy, one can think of a road system: car drivers (functional network) are forced to drive the roads available (structural network), but can still decide which roads to take (Honey et al., 2007; Stam and Reijneveld, 2007). Traffic between brain regions continuously forms dynamic functional networks, even at rest (Eguíluz et al., 2005).

A smart spatial organization, or network *topology*, is important for proper functioning of the functional network. The brain constantly negotiates a trade-

off between low metabolic costs by short connections and high topological efficiency by long connections. In this regard, neurons do not function as isolated units. Assemblies of spatially close neurons interconnect and specialize in certain aspects of functioning. By cooperating their activity, or *synchronizing*, the assemblies communicate and integrate their separate functions into a cognitive operation (Lopes da Silva, 2013; Varela et al., 2001). In other words, higher brain functions comprise a balance between local specialization and global integration of brain processes, mediated by a smart network topology. The functional network thus provides insight into functionally correlated (but spatially distant) brain regions (Bullmore and Sporns, 2009; Fingelkurts, Fingelkurts and Kähkönen, 2005).

Neurological disorders are directly associated with abnormal levels of synchronization, which shows in aberrant network topology (Bullmore and Sporns, 2009; Stam, 2014). Numerous neuroimaging studies showed aberrant resting state functional network topology compared to healthy controls in Alzheimer's disease (Brier et al., 2014), Parkinson's disease (Utianski et al., 2016), schizophrenia (Bullmore and Sporns, 2012) and epilepsy (Garcia-Ramos et al., 2016). Currently, it is not known if mechanisms leading to migraine pathogenesis might show in resting state functional network topology. Studying patterns of resting state activity in the migraine brain therefore provides us with meaningful information about potential abnormalities in the functional network.

Construction of the functional network topology requires three steps (see Figure 1). First, neuronal processes are recorded by a neuroimaging technique, in this case the electroencephalogram (EEG). EEG directly measures neuronal activity and has a high temporal resolution that can capture the fast changing functional network (Bullmore and Sporns, 2009). However, EEG is sensitive to volume conduction, when two electrodes measure activity form the same source (Van Diessen et al., 2015). Second, a tool to quantify synchronization from the recorded brain activity, is provided by *functional connectivity*. Functional connectivity estimates the temporal correlations between anatomically remote neurophysiological signals (in this case EEG time-series). Many methods to estimate functional connectivity have been proposed, each with their pro's and cons (Friston, 2011; David et al., 2004). Lastly, to characterize patterns of functional connectivity and thereby quantify the network topology, a mathematical tool is used: *graph analysis*.

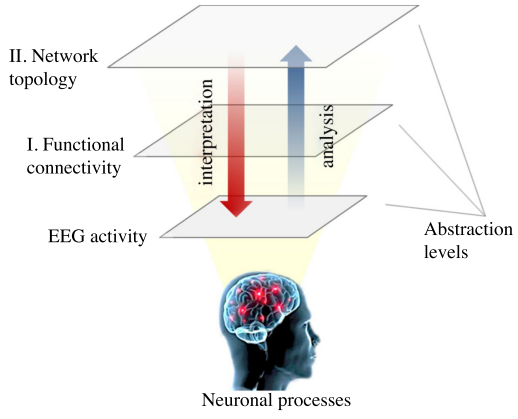

FIGURE 1: Abstraction levels of functional network analysis. New complementary information, which gets more abstract compared to the original neuronal processes, is found with every analysis step (upward arrow). However, an increasing abstraction level results in less intuitive interpretation of the original neuronal processes (downward arrow). Network topology cannot be directly linked to the underlying neuronal processes (image copied from De Vico Fallani et al., 2014).

A graph is an abstract, mathematical representation of a real-world complex network, consisting of nodes (the elements, in this case EEG channels) and edges (the connections between the elements). Edges have weights to represent the strength of connections. Together, nodes and edges form the spatial organization of the network (Bullmore and Sporns, 2012). The quantification of graph measures describing network topology allows for the characterization of efficiency and cost of information transfer in the network. Graph analysis can be applied on any complex network, as these networks typically show similar behavior and share certain organizational principles. Therefore, graph analysis provides quantitative comparison of network topologies in healthy brains and disordered brains (Bullmore and Sporns, 2009).

Although graph analysis of the complete network is helpful for understanding disorder mechanisms, it suffers from methodological issues which might bias comparison between different groups or conditions (Van Wijk et al., 2010). For example, graph measures are influenced by network size (i.e., the number of nodes) and network sparsity (i.e., percentage of edges present). Typically, network size and sparsity differ among individuals, making comparison inconvenient.

An alternative approach to represent brain networks is the *minimum spanning tree* (MST). The MST is a unique, acyclic subgraph of the complete graph, in which the sum of weights is minimized. The MST always has N nodes and $N-1$ edges, making direct comparison among networks possible and avoiding aforementioned issues (Stam et al., 2014; Tewarie et al., 2015). Furthermore, if the original graph possesses strong fluctuations in its edge weights, known as a *strong disorder limit*, most information transport flows over the MST (Van Mieghem and Van Langen, 2005). In terms of the road system, the MST in the strong disorder limit is comparable to a subnetwork of local roads interconnected by highways.

The goal of the current study was to examine the

functional network topology in migraine patients using eyes-closed EEG resting state data. Analyses were performed only on alpha-band (8-13 Hz) data, as the alpha rhythm dominates in eyes-closed resting state EEG recordings (Van Diessen et al., 2015). Based on the assumption of hyperexcitability, it was hypothesized that the functional network is affected in migraine. The main objective was to investigate differences in functional network topology between migraine patients in the interictal state and healthy controls. This was done using MST measures on both a global level and a local node level. An intermediate cluster level was examined with sub-averages of functional connectivity in five predefined clusters of nodes. Furthermore, the influence of volume conduction was examined by using two different functional connectivity methods, one of which accounted for the effect of volume conduction.

2. METHODS

2.1. Participants

We included two groups of participants: 15 healthy controls (age 42.67 ± 19.32; 12 women) and 18 episodic[1] migraine patients in the interictal state (age 38.56 ± 11.50; 16 women). The sample characteristics of the migraine group can be found in Table 1. The inclusion criteria for migraine patients were based on the International Classification of Headache Disorders III guidelines. The study was approved by the Medical Ethics Committee of Leiden University Medical Center. All participants gave written informed consent prior to the experiment.

2.2. Protocol

EEG was recorded in the resting state. Participants lay on a bed with their head resting on a pillow, in a sound-attenuated and electrically shielded room. The participants were instructed to stay awake during the recording and think of nothing in particular. To avoid muscle and eye movement artefacts, participants were asked to lie still and concentrate their gaze to a designated point. The recording paradigm consisted of four blocks of 30 seconds eyes-open and 120 seconds eyes-closed, to prevent drowsiness. This resulted in 8 minutes of eyes-closed data per participant.

2.3. EEG recordings and preprocessing

EEG was recorded using a 128-channel cap (according to the 5/10 systems, by WaveGuard, ANT^{TM} Neuro with Ag/AgCl electrodes) with the left mastoid as reference. Channels M1 and M2 (see Appendix A) were not used during recording. All electrodes were prepared to have an impedance below 20 kΩ. Data were digitized at a sampling rate of 2048 Hz (Refa amplifier, TMSi, Oldenzaal, the Netherlands) and stored for offline analysis. Custom written scripts in MATLAB R2016b (The MathWorks, Inc.) were used for further processing and analyses of the EEG data.

TABLE 1: Sample characteristics of the migraine group (n=18).

	Mean (SD)
Age (years)	38.56 (11.50)
Migraine duration (years)	24.87 (12.82)
Number of attacks (p/month)	1.92 (0.71)
Migraine days (p/month)	3.25 (1.71)
Sex ratio (women:men)	8:1
Migraineurs with aura	6

Continuous EEG data were low pass filtered to prevent aliasing at 70 Hz using a zero-phase fifth-order Butterworth filter, and downsampled to 512 Hz. A 1 Hz high pass zero-phase fifth-order Butterworth filter was applied to remove slow drifts. To remove 50 Hz line noise, the data were band-pass filtered with a second-order infinite impulse response notch filter. The following 21 channels were excluded from further analyses, as scalp contact at these locations was suboptimal in most participants: Fp1, Fpz, Fp2, AF7, AF8, F7, F8, FT7, FT8, FT9, FT0, FTT9h, FTT10h, T7, T8, TP7, TP8, TPP9h, TPP10h, P9 and P10 (see Appendix A). Hence, 105 channels remained for further analysis.

The data were then divided into non-overlapping 4096 sample (8s) epochs. The epochs were visually inspected and 8 artefact-free epochs (a total of 64s) were selected using predefined criteria. These criteria were: 1) the first and last epochs in each of the four eyes-closed blocks are not selected to avoid transitions from closing/opening of the eyes; 2) epochs with obvious (muscle) artefacts are not selected; 3) epochs early in the recording are preferred to prevent the risk of drowsiness; 4) epochs with apparent alpha-band (8-13 Hz) activity are preferred; and 5) epochs without bad channels (i.e., low-quality or missing signals) are preferred to prevent loss of information. A second researcher evaluated the selected epochs, to improve reliability of epoch selection.

Before the selected epochs were extracted for further data analysis, the continuous EEG data were rereferenced to common average. The common average constituted all channels except bad channels. Lastly, bad channels were spherically interpolated by combining signals from neighboring electrodes. In two datasets, a total of six channels were interpolated: CP6 and P8 in one dataset and POO9h, CCP5h, CPP5h and CP2 in another dataset. Continuous EEG data were then filtered in the alpha-band (8-13 Hz) using

[1]Episodic migraine is characterized by those with migraine who have 0 to 14 headache days per month (International Classification of Headache Disorders III)

high and low pass zero-phase fifth-order Butterworth filters. Finally, the selected epochs were extracted from the band-pass filtered data and used for construction of the functional network.

2.4. Data processing

Spectral power was calculated in the continuous EEG epochs of all participants included in the analysis using Fast Fourier Transform. Per epoch, power was averaged across the 105 EEG channels. The average group results can be seen in Figure 2. The power spectra confirmed that analysis of alpha band (8-13 Hz) activity was appropriate.

Per participant, the construction of the functional network was twofold (see Figure 3). First, functional connectivity was calculated per epoch between all possible pairs of 105 EEG channels. The eight resulting epoch-based matrices were averaged and represented in a single 105x105 matrix. Second, the minimum spanning tree was constructed based on the average functional connectivity matrix. This procedure was done for two different methods of functional connectivity.

I Functional connectivity analysis

Functional connectivity was estimated with two different methods: *spectral coherence* and *phase-lag index*. This was done to account for the effect of volume conduction on data analysis. Both methods are based on the phase difference between two signals. To obtain time-varying estimates of phase, a complex component of the signal is needed. Therefore, the complex signal was extracted from the band-pass filtered EEG time-series using the Hilbert transform (Cohen, 2014).

Spectral coherence

Spectral coherence is a measure of synchronization between two signals based on the consistency of their phase differences. Even though two signals may have different phases, coherence will be high if the phase difference between the signals remains constant. In other words, coherence estimates whether two signals can be related by a linear time-invariant transformation. Coherence is always real-valued between 0 and 1, with 0 indicating no relationship and 1 indicating a constant phase difference. High coherence between two EEG signals indicates a linear relationship, even though this does not imply that the underlying cortical dynamics are linear. Despite its fast and easy computation, coherence can detect only linear relationships between time-series (David et al. (2004), Van Diessen et al. (2015)). Coherence was calculated between all pairs of data channels using equation 1:

$$\gamma_{xy}^2 = \frac{|S_{xy}|^2}{S_{xx}S_{yy}} \tag{1}$$

in which S_{xy} is the cross-spectral density of signals x and y (here, time-series of different electrodes) and S_{xx} and S_{yy} are the corresponding auto-spectral densities. A more elaborate explanation of coherence can be found in Appendix B.

Phase-lag index

Like coherence, the phase-lag index (PLI) is based on the phase angle differences between two signals. However, the PLI accounts for volume conduction, when two electrodes measure activity from the same source. The signals of two volume-conducted electrodes will have phase-lags of either zero or π. Therefore, their phase angle differences will be distributed around zero or π radian on the imaginary axis of the complex plane. PLI values will be high if the phase angle differences are predominantly distributed on one side of the imaginary axis. In contrast, if half of the phase angle differences are positive and half are negative with respect to the imaginary axis, the phase-lag index will be zero (Stam, Nolte and Daffertshover, 2007; Cohen, 2014). PLI is calculated by equation 2:

$$PLI_{xy} = \left| n^{-1} \sum_{t=1}^{n} sgn(imag(S_{xy_t})) \right| \tag{2}$$

in which n is the total number of time points in the epoch and $sgn(imag(S_{xy_t}))$ indicates the sign of the imaginary part of the cross-spectral density at time point t.

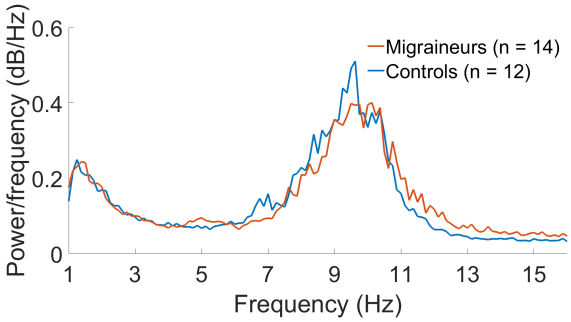

FIGURE 2: Power spectra averaged across 105 EEG scalp channels for the migraine and the control group.

Cluster analysis

Functional connectivity strength was calculated to assess differences between groups in two ways: first, by means of the connection strength of the whole FC matrix and second, by the connection strength in predefined clusters (frontal, central, left, right and occipital (see Figure 4))[2]. The connection strength in predefined clusters included sub-averages of all electrodes participating within those clusters. For example, the average connection strength of the central-occipital cluster is the average of functional connectivity

[2] A bigger version of the 128 EEG channel layout can be found in Appendix A.

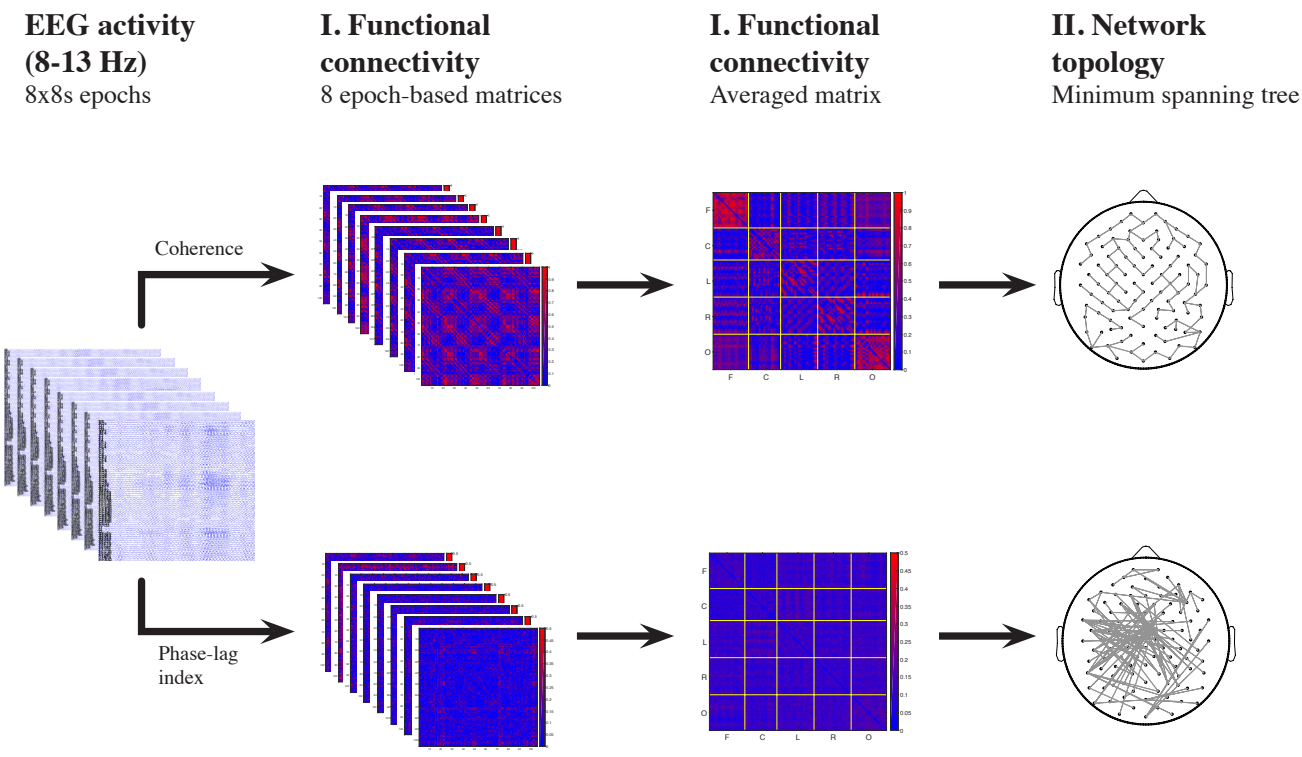

FIGURE 3: Data processing pipeline per participant. Based on 8 epochs (each of 4096 samples, or 8 seconds) of alpha-band data, the functional network was constructed. First, functional connectivity was calculated per epoch between all possible pairs of 105 EEG channels. The 8 resulting functional connectivity matrices were then averaged, out of which the minimum spanning tree was constructed. This procedure was done for two functional connectivity methods per participant.

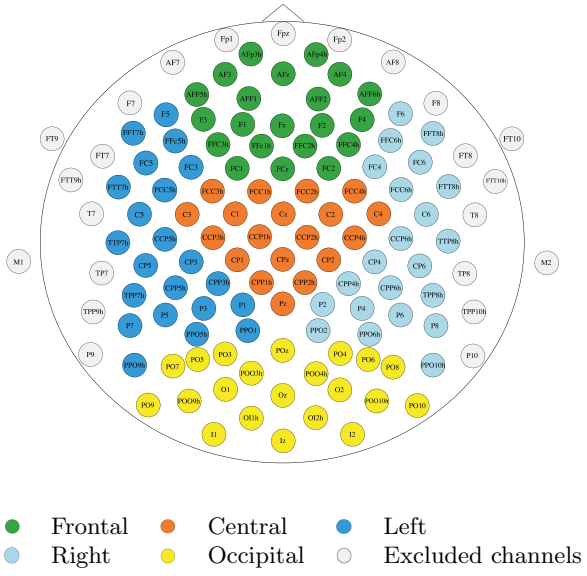

FIGURE 4: Overview of the 128-channel EEG cap. Colors indicate which nodes belong to which cluster. Gray nodes were excluded from analyses, as scalp contact at these positions was suboptimal in most participants.

values of the 21 channels of the frontal cluster with the 19 channels of the central cluster.

II Minimum spanning tree analysis

The minimum spanning tree (MST) is a subgraph of the complete weighted graph (i.e., the functional connectivity matrix in graph form) that connects all nodes without forming loops, while minimizing the sum of edge weights. Nodes represent the EEG channels, while edge weights represent the connections between them. In the MST, the most important edges in the network are the ones represented by low weight. In the current study, however, the most important edges represent the strongest connections, i.e. the highest weights. For the computation of the MST, we therefore defined the edge weight as 1/(functional connectivity estimate) (Tewarie et al., 2015; Stam et al., 2014).

MST's were constructed with Kruskal's algorithm. The algorithm first arranges edge weights (in this case 1/(functional connectivity values)) in ascending order. The construction of the MST starts with the lowest link weight, after which the following lowest link weights are added until all nodes are connected. Once a link forms a cycle in the network, the link is discarded. This results in an acyclic subgraph in which all nodes N are connected by $m = N - 1$ links. It follows

TABLE 2: Summary of global and local minimum spanning tree measures.

	Name	Explanation	Equation
N	Nodes	Number of nodes	
m	Links	Number of links	
k	Degree	Number of links per node	$k_i = \sum a_{ij}$, in which a_{ij} is the adjacency matrix
BC	Betweenness centrality	Fraction of paths that pass through a given node	$BC_i = \frac{1}{(N-1)(N-2)} \sum_{s \neq v \neq t} \frac{\sigma_{st}^{(v)}}{\sigma_{st}}$, in which σ_{st} is the number of shortest paths between node s and node t and $\sigma_{st}^{(v)}$ are the shortest paths between s and t that pass through node v
E	Eccentricity	Longest path of a given node	$E_i = (d_{ij})_{max}$, in which d_{ij} is the length of the path from node i to node j
L_f	Leaf fraction	Fraction of nodes L with only one link ($k = 1$)	$L_f = L/N$
D	Diameter	Longest of all paths (d) in the graph	$D = d/m$
T_h	Tree hierarchy	The trade-off between large scale integration and maximum betweenness centrality	$T_h = \frac{L}{2mBC_{max}}$
r	Degree correlation	Correlation between the degree of a node and the degrees its neighboring nodes (to which it is connected)	$r = \sum_{jk} \frac{jk(e_{jk} - q_j q_k)}{\sigma^2}$, in which $\sigma^2 = \sum_k k^2 q_k - [\sum_k k q_k]^2$ see Appendix C for more information
O	Overlap	The fraction of links that two MST's have in common	$O = \frac{MST_x \cap MST_y}{m}$

from the algorithm that two conditions must be met when constructing the MST: all nodes in the complete, weighted graph are connected and all edge weights are unique (Van Mieghem and Van Langen, 2005).

After construction of the MST, all edges were assigned an equal weight for the sake of proper comparison between groups. The resulting matrix is called the adjacency matrix. To quantify the topology of MST's, both global and local properties were examined. All measures are summarized in Table 2.

Local MST measures

Local MST measures indicate node importance within the network topology and are calculated for each node separately. In Figure 5, three examples of tree topologies with equal number of nodes are given. Three local MST metrics were examined in this study: degree (k), betweenness centrality (BC) and eccentricity (E). The degree of a node is the number of links connecting to that node. The path-like tree in Figure 5, consists of two nodes with degree one, and seven nodes with degree two. The star-like topology on the other hand, has one highly connected node (degree eight) and eight *leaf nodes* (nodes with $k = 1$). The betweenness centrality is the fraction of paths a given node participates in, between any two nodes in the network. The central node in the star-like topology in Figure 5, for example, participates in every path between any pair of its neighboring leaf nodes and therefore has a BC of one. The nodes with the highest BC carry the highest load. Finally, eccentricity is defined as the longest path of a given node. The blue nodes in Figure 5, have eccentricities of four (path-like tree), two (hierarchical tree) and one (star-like tree). The lower the eccentricity, the more central the node is (Tewarie et al., 2015; Stam et al., 2014). Here, eccentricity is normalized by the amount of links m and degree by the amount of nodes N. Local measures were characterized by means of critical nodes (maximum degree, maximum betweenness centrality and minimum eccentricity).

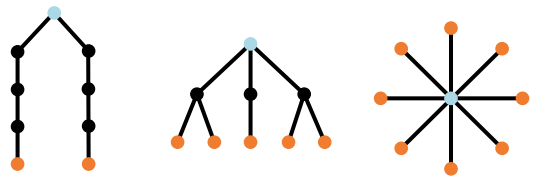

(a) Path-like (b) Hierarchical (c) Star-like

FIGURE 5: Examples of minimum spanning tree topologies. Blue nodes are the most central nodes, orange nodes are leafs (degree one). The path-like tree (a) and the star-like tree (c) represent two extreme shapes. The hierarchical tree (b) is situated in between those extremes.

Global MST measures

Global measures of MST topology provide information on the large scale integration of the network. Four global MST properties were examined in this study: leaf fraction (L_f), diameter (D), tree hierarchy (T_h) and degree correlation (R). The leaf fraction is the fraction of leafs (L) in the network. The number of leafs has a lower bound of 2 and an upper bound of $N - 1$. The

diameter of the network is the longest path between any two nodes in the tree. Diameter is related to leaf fraction by $d = m - L + 2$
in which m is the total number of links and L is the number of leaf nodes.

Figure 5 implies that the star-like topology results in efficient network communication; that is, all pairs of nodes are either one or two links apart. High global efficiency therefore requires a small diameter (i.e., many leaf nodes). A star-like topology, however, also is highly vulnerable due to high BC of the central node. Failure of this node will disrupt all communication in the network. A balance between diameter reduction and overload prevention (high BC comes with high load), captures an optimal configuration. This trade-off is reflected by tree hierarchy in equation 3:

$$T_h = \frac{L}{2mBC_{max}} \tag{3}$$

in which L is the number of leaf nodes, m is the total number of links and BC_{max} is the maximum betweenness centrality. The denominator is multiplied by 2 to assure that T_h ranges between 0 and 1. In the case of a path (i.e., $L = 2$ and m approaches infinity), $T_h = 0$ and in case of a star (i.e., $L = m$), $T_h = 0.5$ (Tewarie et al., 2015; Stam et al., 2014).

Degree correlation indicates whether the degree of a node is correlated with the degrees of its neighboring nodes. A positive degree correlation indicates that nodes prefer to connect to other nodes with the same or similar degrees. The tree is then called assortative (Stam and Van Straaten, 2012; Bullmore and Sporns, 2009; Newman, 2002). Finally, overlap is the fraction of links that two MST's have in common. Here, the overlap between all MST's of the migraine group compared to the backbone MST of the control group (based on the mean functional connectivity matrix of that group) was calculated, and vice versa.

Strong disorder limit
The MST is the critical backbone of the complete, weighted graph only under the condition of a *strong disorder limit*. If the link weights in the complete graph show strong variations, then the sum of weights (by which the MST is constructed) will be dominated by a single weight. The link weights then possess a strong disorder limit. If this condition holds, then most information flow goes over very few backbone links: the MST (Van Mieghem and Van Langen, 2005).

The weight distribution (F_w) of the complete graph can be described by the polynomial distribution in equation 4:

$$F_w(x) = \begin{cases} x^\alpha & \text{if } 0 \le x \le 1 \\ 1 & \text{if } x > 1 \end{cases} \tag{4}$$

in which x represents the weights (in our case either coherence or PLI values) and α is called the *extreme value index*. A strong disorder limit occurs when $\alpha \to 0$. A decreasing α corresponds to an increasing probability that shortest paths of the complete graph coincide with the MST (Tewarie et al., 2014).

For regular graphs[3], there is a critical $\alpha_c > 0$ for which $\alpha < \alpha_c$ indicates the critical backbone of the complete network (i.e., $\alpha \to 0$). According to Van Mieghem and Van Langen (2005), $\alpha_c = O(m^{-2})$, in which m are the number of links in the network. We will use the same criterion as a threshold for the strong disorder limit in this study. Therefore, with $m = 104$, $\alpha_c \approx 0.0001$.

From the complete graph (i.e., the functional connectivity matrix), for every participant separately, we ranked the weights of all matrix elements in descending order and estimated α from this distribution, using a power function $f(x) = ax^\alpha + b$.

2.5. Statistics

Global and local differences in network topology, as well as cluster-level differences in functional connectivity strength between migraineurs and controls were assessed using Mann-Whitney U-tests. None of the data were normally distributed or met the assumption of homogeneity of variance. Therefore, a nonparametric test was chosen for all measures. A value of $p < 0.05$ was considered significant.

3. RESULTS

Data from seven participants (four migraineurs and three controls) were excluded from analysis; one participant experienced migraine within three days after recording and was therefore not in the interictal state; three data sets were unusable due to recording issues (a broken ground electrode, a high noise level and problems with data storing); and eyes closed data in two participants were contaminated by regular artefacts (eye blinking and heartbeats).

Functional connectivity
Connectivity strength was calculated in two ways. First, the mean strength of all 105 channels was calculated for every participant and compared between migraineurs and controls. Second, sub-averages in five predefined clusters (frontal, central, left, right and occipital) were calculated within and between clusters for every participant and compared between groups. This was done for both functional connectivity methods (coherence and PLI). Typical functional connectivity matrices, based on the mean functional connectivity per group, can be seen in Figure 6. The results of the Mann-Whitney U-tests for assessing differences between groups are presented Table 3. No significant differences were found in mean connectivity strength (including all channels) for both functional connectivity

[3]Regular graphs are graphs in which each node has the same degree

TABLE 3: Functional connectivity (sub-)averages based on coherence and phase-lag index in the alpha band (8-13 Hz). No significant differences were found between migraineurs and controls ($p<0.05$). Number of channels per cluster: Frontal (n=21), Central (n=19), Left (n=22), Right (n=22), Occipital (n=21).

	COHERENCE			PHASE-LAG INDEX		
Cluster	**Migraineurs Mean (SD)**	**Controls Mean (SD)**	**p-value**	**Migraineurs Mean (SD)**	**Controls Mean (SD)**	**p-value**
All	0.42 (0.11)	0.36 (0.07)	0.16	0.22 (0.10)	0.21 (0.09)	0.86
Frontal - Frontal	0.80 (0.11)	0.76 (0.12)	0.34	0.18 (0.06)	0.17 (0.08)	0.52
Frontal - Central	0.40 (0.12)	0.37 (0.15)	0.59	0.25 (0.12)	0.23 (0.13)	0.77
Frontal - Left	0.41 (0.13)	0.36 (0.12)	0.46	0.22 (0.09)	0.19 (0.10)	0.42
Frontal - Right	0.48 (0.16)	0.39 (0.11)	0.14	0.21 (0.09)	0.20 (0.07)	1.00
Frontal - Occipital	0.57 (0.15)	0.51 (0.13)	0.32	0.23 (0.11)	0.23 (0.10)	0.91
Central - Central	0.43 (0.07)	0.46 (0.09)	0.49	0.21 (0.09)	0.20 (0.09)	0.82
Central - Left	0.30 (0.07)	0.28 (0.08)	0.46	0.21 (0.09)	0.20 (0.10)	0.60
Central - Right	0.33 (0.11)	0.29 (0.08)	0.27	0.23 (0.11)	0.21 (0.08)	0.91
Central - Occipital	0.42 (0.12)	0.41 (0.11)	0.66	0.23 (0.11)	0.22 (0.10)	0.73
Left - Left	0.38 (0.05)	0.36 (0.05)	0.14	0.21 (0.10)	0.17 (0.09)	0.38
Left - Right	0.34 (0.08)	0.29 (0.07)	0.13	0.21 (0.10)	0.18 (0.07)	0.69
Left - Occipital	0.36 (0.10)	0.32 (0.10)	0.19	0.22 (0.10)	0.21 (0.10)	0.82
Right - Right	0.44 (0.11)	0.37 (0.05)	0.05	0.22 (0.10)	0.20 (0.07)	0.82
Right - Occipital	0.41 (0.16)	0.32 (0.10)	0.13	0.23 (0.11)	0.22 (0.08)	0.91
Occipital - Occipital	0.54 (0.12)	0.50 (0.09)	0.40	0.22 (0.11)	0.23 (0.09)	0.45

Note: SD= standard deviation

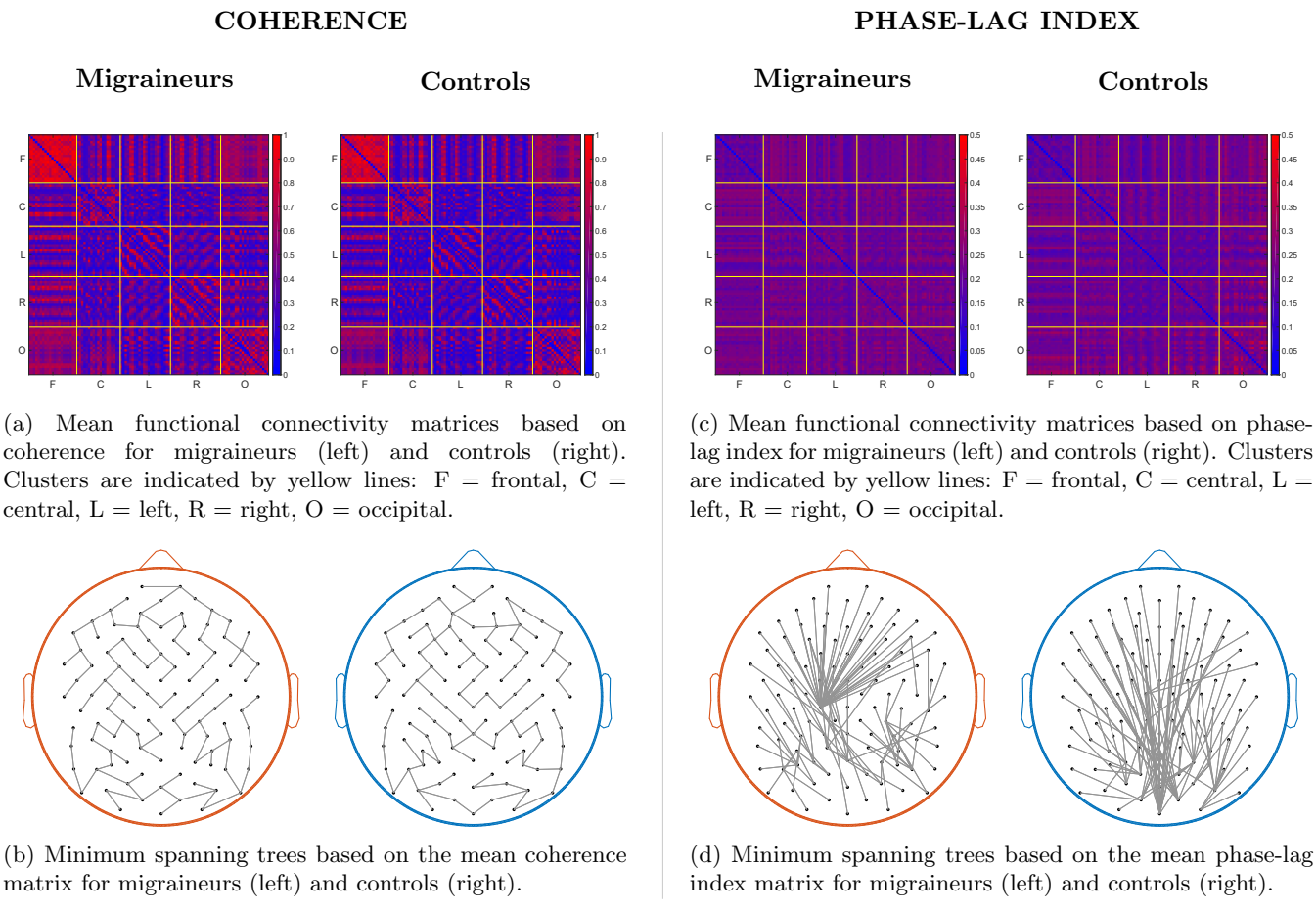

(a) Mean functional connectivity matrices based on coherence for migraineurs (left) and controls (right). Clusters are indicated by yellow lines: F = frontal, C = central, L = left, R = right, O = occipital.

(b) Minimum spanning trees based on the mean coherence matrix for migraineurs (left) and controls (right).

(c) Mean functional connectivity matrices based on phase-lag index for migraineurs (left) and controls (right). Clusters are indicated by yellow lines: F = frontal, C = central, L = left, R = right, O = occipital.

(d) Minimum spanning trees based on the mean phase-lag index matrix for migraineurs (left) and controls (right).

FIGURE 6: Functional connectivity matrices based on the mean functional connectivity per group for coherence (a) and phase-lag index (c). The corresponding minimum spanning trees are shown for coherence (b) and phase-lag index (d).

methods. Furthermore, no significant differences were found within or between clusters between groups for both connectivity methods. The group effect of the right within-cluster in coherence just fell short of significance (p = 0.05). However, after Bonferroni correction to correct for multiple comparisons ($p < \frac{0.05}{15}$), the group effect of the right within-cluster in coherence was far from significant.

MST measures
To quantify the functional network, measures of the minimum spanning tree (MST) were calculated on both a global and a local network level for every participant. Typical MST's, based on the mean functional connectivity matrices per group, can be seen in Figure 6. Global MST measures yielded no significant differences between groups for both functional connectivity methods (see Table 4). Local MST measures were calculated per node and mean distributions per group are visualized in Figure 7. No significant differences were found in the distributions of the local MST measures between groups for both functional connectivity methods. Furthermore, no significant differences were found in maximum degree, maximum betweenness centrality and minimum eccentricity between groups for both functional connectivity methods (see Table 4). The collection of critical nodes per group are shown in Figure 8. Minimum spanning trees including critical nodes per participant are shown in Appendix D. The amount of overlap was similar in both groups (see Table 4). Overlapping links within groups are shown in Appendix E.

Strong disorder limit
The MST forms the critical backbone of the complete graph only if the weight distribution possesses a strong disorder limit. For each participant, we estimated the extreme value index α in its weight distribution. The results can be seen in Figure 9. For all participants, the weight distributions had a value of α between 0.12 and 1.61. Therefore, none of the weight distributions possess strong disorder limit ($\alpha_c \approx 0.0001$).

4. DISCUSSION

The present study examined the topological organization of brain networks in episodic migraine patients and healthy controls by applying minimum spanning tree (MST) analysis to eyes closed resting state EEG data. This was done based on two different functional connectivity methods to account for the effect of volume conduction. For both functional connectivity methods, no significant differences were found in the MST; neither on a global level, nor on a local level. Furthermore, no significant differences were found in functional connectivity strength. In contrast with the hypothesis, the results indicate that the interictal resting state functional networks (RSFN) of migraine patients and healthy controls are not different.

Clinical interpretation
Our finding is in accordance with the only similar graph-based resting state study in migraine patients by Wu et al. (2016). With eyes-closed magnetoencephalography (MEG) data, they investigated the complete graphs of migraineurs (with and without aura) and healthy controls. Wu et al. (2016) found no significant differences in topological organization, nor in functional connectivity strength based on coherence between groups in the alpha band (8-12 Hz). This study supports the idea that the interictal migraine functional network might not function abnormally in the resting state.

However, multiple findings argue in favor of permanent abnormalities in the migraine RSFN. Firstly, studies based on resting state functional magnetic resonance imaging (rs-fMRI) found increased connectivity in specific brain areas in the RSFN of migraineurs compared to healthy controls, especially in pain-processing areas (Sprenger and Magon, 2013; Maneiro, Boshyan and Hadjikhani, 2011). The advantage of fMRI over EEG and MEG is a high spatial resolution, in the order of millimeters. In EEG and MEG, only activity in the upper layer of the cortex is recorded. Abnormalities in the migraine RSFN might be highly localized and not detectable with EEG- or MEG-based graph analysis. Possibly, brain dysfunction is attributed to the level of neuronal assemblies and not to abnormal network connectivity.

Furthermore, interictal migraine network topology might be comparable to that of epilepsy. Migraine and epilepsy follow the same sequence in attacks (defined by phases before (preictal), during (ictal) and after (postictal) attacks) and are believed to have pathophysiological overlap (Nye and Thadani, 2015). In some patients, the disorders occur comorbidly and are linked genetically. Like migraine, epilepsy originates from electrical disturbances in the brain and attacks are unforeseen and unprovoked. Accordingly, many epilepsy graph-based resting state studies found abnormal network topology in the interictal state compared to the ictal state and/or healthy controls (Ponten et al., 2007; Van Dellen et al., 2009; Garcia-Ramos et al., 2016). The interictal epilepsy network might be organized in such a way that it facilitates an increased tendency to synchronize. This advocates that the interictal migraine functional network might be abnormal in the resting state too.

It is currently not known if functional connectivity and topological organization are abnormal in the preictal, ictal or postictal migraine states. Future neuroimaging studies should investigate whether migraine patients show abnormal interictal network topology when compared to other states. Furthermore, the interictal RSFN might differ between migraineurs with and without aura (Hougaard et al., 2015). Future research

TABLE 4: Minimum spanning tree measures in the alpha band (8-13 Hz). No significant differences were found between migraineurs and controls ($p<0.05$).

	COHERENCE			PHASE-LAG INDEX		
MST measure	**Migraineurs Mean (SD)**	**Controls Mean (SD)**	**p-value**	**Migraineurs Mean (SD)**	**Controls Mean (SD)**	**p-value**
Leaf fraction	0.32 (0.05)	0.31 (0.04)	0.86	0.73 (0.09)	0.71 (0.08)	0.62
Diameter	0.35 (0.05)	0.32 (0.07)	0.22	0.13 (0.04)	0.12 (0.04)	0.66
Tree hierarchy	0.52 (0.08)	0.52 (0.07)	0.95	1.00 (0.14)	0.95 (0.12)	0.45
Degree correlation	-0.23 (0.10)	-0.18 (0.09)	0.32	-0.43 (0.11)	-0.38 (0.11)	0.52
Max. degree	4.08 (0.29)	4.57 (1.50)	0.61	22.79 (8.08)	21.08 (8.20)	0.62
Max. BC	0.31 (0.03)	0.30 (0.02)	0.80	0.37 (0.03)	0.37 (0.03)	1.00
Min. eccentricity	0.17 (0.03)	0.16 (0.03)	0.23	0.07 (0.02)	0.07 (0.02)	0.94
Overlap	0.59 (0.08)	0.60 (0.05)	0.84	0.04 (0.03)	0.04 (0.03)	0.53

Note: SD = Standard deviation

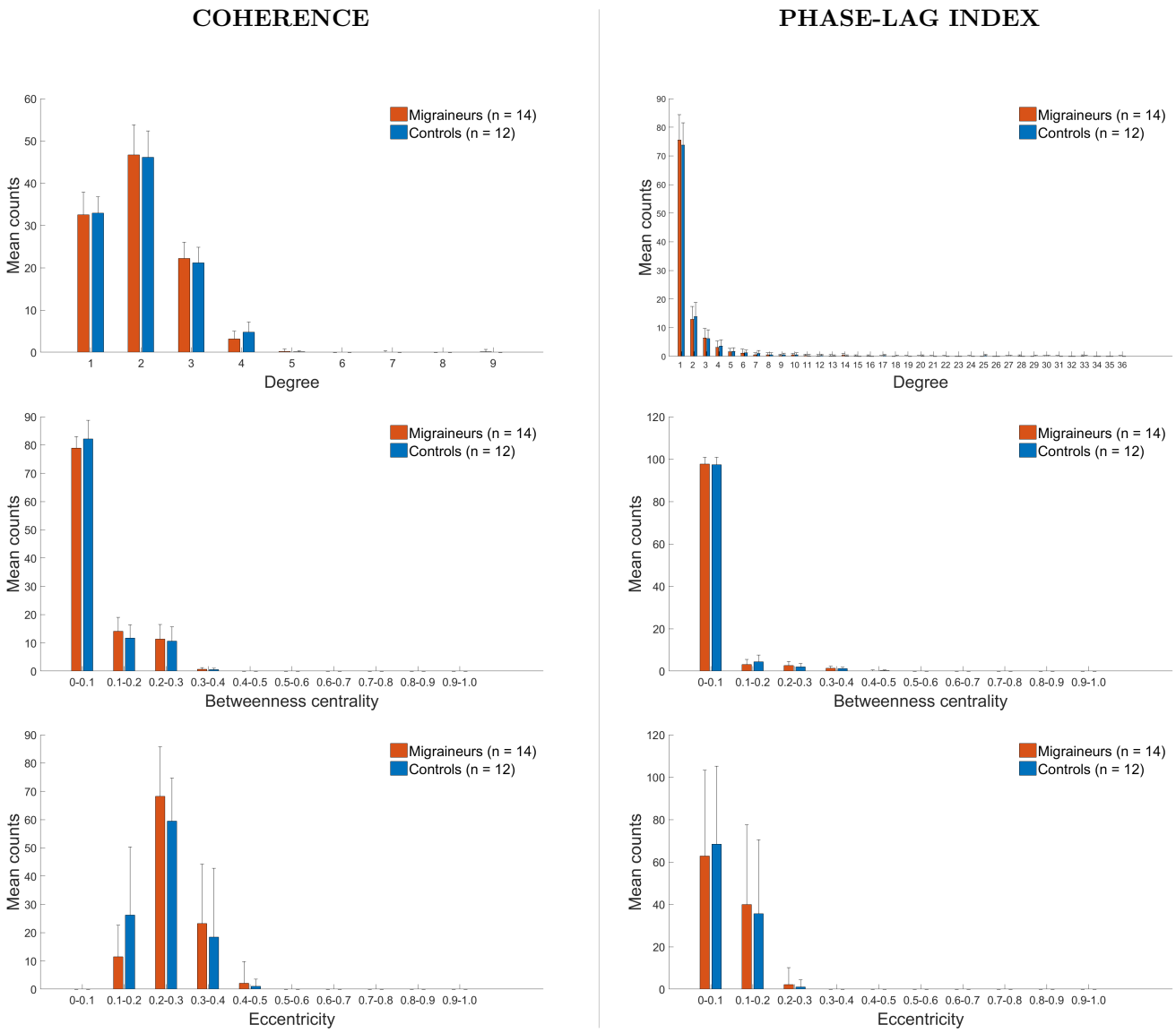

FIGURE 7: Distributions of local minimum spanning tree measures based on coherence (left side) and phase-lag index (right side). All distributions show the mean and standard deviation of migraineurs (orange) and controls (blue).

FIGURE 8: Totality of critical nodes based on coherence (left side) and phase-lag index (right side) in migraineurs (orange) and controls (blue). The colors of the dots indicate counts of a critical nodes, if the particular node appeared in more than one participant.

should elucidate the effect of aura on the RSFN. Lastly, a combination of fMRI (with high spatial resolution) and EEG (with high temporal resolution) recordings might give complementary information and therewith provide more accurate results.

Data interpretation

The functional connectivity measure is of major influence on the shape of the MST. Both coherence and PLI detect coupling in EEG time series, but with different sensitivity profiles; coherence is able to detect only linear coupling, while PLI detects weak and nonlinear coupling (David et al., 2004), and accounts for volume conduction (Stam, Nolte and Daffertshover,

2007). However, in epilepsy, measures affected by volume conduction better discriminate between the preictal and ictal state (Christodoulakis et al., 2014). Choice of functional connectivity measure therefore depends on the research objective.

Comparison between the topological organizations of the coherence-based MST and the PLI-based MST clearly reveals the effect of volume conduction (see Figure 6). In the coherence-based MST, network topology was dominated by local connections between neighboring channels. Such local connections were not present in the PLI-based MST, which was dominated by long distance connections. Functional connectivity for neighboring channels might strongly be influenced by volume conduction in coherence-based MST's. This might also explain the higher amount of overlapping links in coherence compared to PLI.

Based on the constant trade-off between metabolic costs and topological efficiency due to functional segregation and functional integration in the human brain, the MST is expected to show star-like as well as path-like characteristics, like a hierarchical tree (Tewarie et al., 2014). Coherence-based MST's showed a hierarchical tree with path-like branches, while MST's based on phase-lag index showed a hierarchical tree with typical star-like characteristics. PLI-based MST's were characterized by some high-degree nodes and many leaf nodes (k=*1*), typical for star-like trees. The degree distribution in coherence showed a peak at $k = 2$, which is typical for a tree with a filamentary structure, or longer "branches" (Lovelace Rainbolt and Schmitt, 2017). T_h in PLI was close to 1 for both groups, suggesting an optimal combination of short distances and prevention of overload of any node.

Critical nodes were assessed to visualize local MST measures. Most critical nodes were expected in the occipital cortex, as alpha-band activity predominantly originates from here during wakeful relaxation with eyes-closed (Van Diessen et al., 2015; Liu et al., 2015).

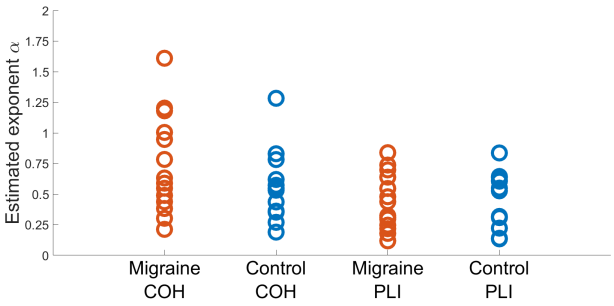

FIGURE 9: Estimated exponent alpha. Link weights of the complete network possess a strong disorder limit if $\alpha < 0.0001$. In this case, alpha ranges between 0.12 and 1.61 for both groups based on coherence (COH) and phase-lag index (PLI).

In coherence-based MST's, critical nodes were scattered throughout the EEG electrodes in both groups, possibly due to the effect of volume conduction (see Figure 8). Contrarily, in PLI-based MST's, most critical nodes originated from the occipital/central part in the control group. In the migraine group, PLI-based critical nodes were more scattered. Considering the fact that the migraine RSFN might show abnormalities only on a local level, the location of critical nodes should be investigated more thoroughly in future MST analyses.

Influence of the strong disorder limit

MST topology, and thereby MST measures, depend only on the ranking of link weights of the complete graph and not on the absolute values or distribution of those weights. The MST is robust only if link weights possess strong variations; otherwise, slight changes in link weight could result in substantially different MST topology (Stam et al., 2014). Merely a comparison of MST measures between groups, might therefore not be conclusive. The distribution of link weights, and especially the strong disorder limit, should be investigated too. Only if the weights of the complete network possess a strong disorder limit, the minimum spanning tree is the critical backbone of the complete weighted network (Van Mieghem and Van Langen, 2005). None of the networks in the current study possessed a strong disorder limit ($0.12 \leq \alpha \leq 1.61$). Therefore, none of the MST's in this study dominated the information flow of the original network. For the comparison of brain networks, the distribution of link weights might be more important than network topology itself; the latter only matters if the MST truly reflects the complete graph.

Most of the minimum spanning trees in the current study possess a *weak disorder limit*; the link weights contribute equally to the sum of weights by which the minimum spanning tree is created (Havlin et al., 2005). Information flow in these networks is spread out over more paths than just the MST, leading to a more balanced overall network load (Van Mieghem and Van Langen, 2005). Since $\alpha_c = O(m^{-2})$, a lower m (number of links) will result in a higher α_c. MST analyses might therefore better reflect underlying activity with 32- or 64-channel EEG.

Methodological issues

In general, many methodological choices are required in EEG-based graph analyses, which may have great influence on results. The choice of reference electrode, artefact handling and filtering, the number and length of epochs and the choice of frequency band can all affect network topology. Furthermore, there is no gold standard in defining nodes and edges. These methodological issues make comparison among studies difficult (Van Diessen et al., 2015).

The present study showed advantages compared to other neuroimaging-based migraine studies. Resting state recordings are simple and not harmful to

participants, while stimulation studies have a complex design (Diaz et al., 2013; Meisel et al., 2015) and might trigger migraine attacks. Furthermore, the MST is barely affected by epoch length and shows similar results even for very short epochs (Fraschini et al., 2016). The use of MST's makes proper comparison among complex networks possible (Stam et al., 2014).

However, the current study had some methodological issues. The time signals in epochs were assumed to be stationary, while the brain continuously changes configuration on multiple time scales, even in the order of seconds (Bullmore and Sporns, 2012; Honey et al., 2007). Smith et al., 2017 proposed a method for both coherence and phase-lag index to handle dynamic connectivity. Furthermore, the resting state comprises multiple levels of cognition (Diaz et al., 2013; Van Diessen et al., 2015) and it was not verifiable if all participants were in the same state. This might have biased the results. Lastly, graph analysis increases the abstraction level of information and interpretation of MST results cannot be directly related to neuronal dysfunction. Cluster analysis (without the use of predefined clusters) of functional connectivity patterns might give more intuitive results compared to the original neuronal processes. A method for data clustering in MST's can be found in Yu et al. (2015).

5. CONCLUSION

The EEG-based resting state functional network of interictal migraine patients does not show any abnormalities on a global, intermediate or local network level compared to healthy controls. Possibly, abnormalities in resting state are highly localized at the level of individual neurons or neuronal assemblies and do not show on network level. The spatial resolution in EEG might be too low to detect such subtle abnormalities. Even though resting state EEG studies are easy to compute and participants do not experience the resting state as harmful, external stimulation might be necessary to assess differences between the functional networks of migraineurs and controls.

Furthermore, the minimum spanning tree offers an unbiased method for comparison between groups. The effect of volume conduction can clearly be seen in MST topology. However, high density EEG recordings increase the threshold by which the MST is considered the critical backbone of the complete graph. Therefore, a trade-off between spatial resolution of the neuroimaging technique and the resulting number of links in the MST should be accounted for in future MST studies.

REFERENCES

[1] Allen, E. A., Damaraju, E., Plis, S. M., Erhardt, E. B., Eichele, T., and Calhoun, V. D. (2014) Tracking whole-brain connectivity dynamics in the resting state. *Cerebral Cortex*, **24**, 663–676.

[2] Aurora, S. K. and Wilkinson, F. (2007) The brain is hyperexcitable in migraine. *Cephalalgia*, **27**, 1442–1453.

[3] Brier, M. R., Thomas, J. B., Fagan, A. M., Hassenstab, J., Holtzman, D. M., Benzinger, T. L., Morris, J. C., and Ances, B. M. (2014) Functional connectivity and graph theory in preclinical Alzheimer's disease. *Neurobiology of Aging*, **35**, 757–768.

[4] Bullmore, E. and Sporns, O. (2012) The economy of brain network organization. *Nature Reviews Neuroscience*, **13**, 336–349.

[5] Bullmore, E. and Sporns, O. (2009) Complex brain networks: graph theoretical analysis of structural and functional systems. *Nature Publishing Group*, **10**, 186–198.

[6] Christodoulakis, M., Hadjipapas, A., Papathanasiou, E. S., Anastasiadou, M., Papacostas, S. S., and Mitsis, G. D. (2014) On the effect of volume conduction on graph theoretic measures of brain networks in epilepsy. *Modern Electroencephalographic Assessment Techniques: Theory and Applications*, pp. 103–130.

[7] Cohen, M. (2014) *Analyzing Neural Time Series Data: Theory and Practice*, 1 edition. The MIT Press.

[8] David, O., Cosmelli, D., and Friston, K. J. (2004) Evaluation of different measures of functional connectivity using a neural mass model. *NeuroImage*, **21**, 659–673.

[9] Diaz, B. A., Van, S., Sluis, D., Moens, S., Benjamins, J. S., Migliorati, F., Stoffers, D., Den Braber, A., Poil, S.-S., Hardstone, R., Van 't Ent, D., Boomsma, D. I., De Geus, E., Mansvelder, H. D., Van Someren, E. J. W., Linkenkaer-Hansen, K., Sahdra, B., and Mooneyham, B. W. (2013) The Amsterdam Resting-State Questionnaire reveals multiple phenotypes of resting-state cognition. *Frontiers in Human Neuroscience*, **7**, 1–15.

[10] Eguíluz, V. M., Chialvo, D. R., Cecchi, G. A., Baliki, M., and Apkarian, A. V. (2005) Scale-free brain functional networks. *Physical Review Letters*, **94**, 1–4.

[11] Fallani, F. D. V., Richiardi, J., Chavez, M., and Achard, S. (2014) Graph analysis of functional brain networks: practical issues in translational neuroscience. *Phil. Trans. R. Soc. B.*, **1**, 1–17.

[12] Fingelkurts, A. A., Fingelkurts, A. A., and Kähkönen, S. (2005) Functional connectivity in the brain - Is it an elusive concept? *Neuroscience and Biobehavioral Reviews*, **28**, 827–836.

[13] Fraschini, M., Demuru, M., Crobe, A., Marrosu, F., Stam, C. J., and Hillebrand, A. (2016) The effect of epoch length on estimated EEG functional connectivity and brain network organisation. *Journal of Neural Engineering*, **13**, 1–10.

[14] Friston, K. J. (2011) Functional and Effective Connectivity: A Review. *Brain Connectivity*, **1**, 13–36.

[15] Garcia-Ramos, C., Song, J., Hermann, B. P., and Prabhakaran, V. (2016) Low functional robustness in mesial temporal lobe epilepsy. *Epilepsy Research*, **123**, 20–28.

[16] Goadsby, P. J. (2003) Migraine : diagnosis and management. *Internal Medicine Journal*, **33**, 436–442.

[17] Havlin, S., Braunstein, L. A., Buldyrev, S. V., Cohen, R., Kalisky, T., Sreenivasan, S., and Stanley, H. E. (2005) Optimal path in random networks with disorder: A mini review. *Physica A*, **346**, 82–92.

[18] Honey, C. J., Kötter, R., Breakspear, M., and Sporns, O. (2007) Network Structure of Cerebral Cortex Shapes Functional Connectivity on Multiple Time Network structure of cerebral cortex shapes functional connectivity on multiple time scales. *Source: Proceedings of the National Academy of Sciences of the United States of America*, **104**, 10240–10245.

[19] Hougaard, A., Amin, F. M., Magon, S., Sprenger, T., Rostrup, E., and Ashina, M. (2015) No abnormalities of intrinsic brain connectivity in the interictal phase of migraine with aura. *European Journal of Neurology*, **22**, 702–e46.

[20] Liu, J., Zhao, L., Lei, F., Zhang, Y., Yuan, K., Gong, Q., Liang, F., and Tian, J. (2015) Disrupted resting-state functional connectivity and its changing trend in migraine suffers. *Human Brain Mapping*, **36**, 1892–1907.

[21] Lopes da Silva, F. (2013) EEG and MEG: Relevance to neuroscience. *Neuron*, **80**, 1112–1128.

[22] Lovelace Rainbolt, J. L. and Schmitt, M. (2016). The Use of Minimal Spanning Trees in Particle Physics.

[23] M.E.J. Newman (2002) Assortative Mixing in Networks. *Physical Review Letters*, **89**, 1–4.

[24] Mainero, C., Boshyan, J., and Hadjikhani, N. (2011) Altered functional magnetic resonance imaging resting-state connectivity in periaqueductal gray networks in migraine. *Annals of Neurology*, **70**, 838–845.

[25] Meisel, C., Schulze-Bonhage, A., Freestone, D., Cook, M. J., Achermann, P., and Plenz, D. (2015) Intrinsic excitability measures track antiepileptic drug action and uncover increasing/decreasing excitability over the wake/sleep cycle. *Proceedings of the National Academy of Sciences*, **112**, 14694–14699.

[26] Moulton, E. A., Becerra, L., Maleki, N., Pendse, G., Tully, S., Hargreaves, R., Burstein, R., and Borsook, D. (2011) Painful heat reveals hyperexcitability of the temporal pole in interictal and ictal migraine states. *Cerebral Cortex*, **21**, 435–448.

[27] Nye, B. L. and Thadani, V. M. (2015) Migraine and epilepsy: Review of the literature. *Headache*, **55**, 359–380.

[28] Ponten, S. C., Bartolomei, F., and Stam, C. J. (2007) Small-world networks and epilepsy: Graph theoretical analysis of intracerebrally recorded mesial temporal lobe seizures. *Clinical Neurophysiology*, **118**, 918–927.

[29] Rubinov, M. and Sporns, O. (2010) Complex network measures of brain connectivity: Uses and interpretations. *NeuroImage*, **52**, 1059–1069.

[30] Scheffer, M., van den Berg, A., and Ferrari, M. D. (2013) Migraine Strikes as Neuronal Excitability Reaches a Tipping Point. *PLoS ONE*, **8**, 1–4.

[31] Smith, K., Smith, K., Member, S., Spyrou, L., and Escudero, J. (2017). Graph-Variate Signal Analysis : Framework and Applications.

[32] Sprenger, T. and Magon, S. (2013) Can functional magnetic resonance imaging at rest shed light on the pathophysiology of migraine? *Headache*, **53**, 723–725.

[33] Stam, C. J. and Van Straaten, E. C. W. (2012) The organization of physiological brain networks. *Clinical Neurophysiology*, **1**, 167–1087.

[34] Stam, C., Tewarie, P., Van Dellen, E., van Straaten, E., Hillebrand, A., and Van Mieghem, P. (2014) The trees and the forest: Characterization of complex brain networks with minimum spanning trees. *International Journal of Psychophysiology*, **92**, 129–138.

[35] Stam, C. J. (2014) Modern network science of neurological disorders. *Nature Reviews Neuroscience*, **15**, 683–695.

[36] Stam, C. J., Nolte, G., and Daffertshofer, A. (2007) Phase lag index: Assessment of functional connectivity from multi channel EEG and MEG with diminished bias from common sources. *Human Brain Mapping*, **28**, 1178–1193.

[37] Stam, C. J. and Reijneveld, J. C. (2007) Graph theoretical analysis of complex networks in the brain. *Nonlinear Biomedical Physics*, **1**, 1–19.

[38] Tewarie, P., Hillebrand, A., Schoonheim, M. M., Van Dijk, B. W., Geurts, J. J. G., Barkhof, F., Polman, C. H., and Stam, C. J. (2014) Functional brain network analysis using minimum spanning trees in Multiple Sclerosis: An MEG source-space study. *NeuroImage*, **88**, 308–318.

[39] Tewarie, P., van Dellen, E., Hillebrand, A., and Stam, C. J. (2015) The minimum spanning tree: An unbiased method for brain network analysis. *NeuroImage*, **104**, 177–188.

[40] Utianski, R. L., Caviness, J. N., Van Straaten, E. C. W., Beach, T. G., Dugger, B. N., Shill, H. A., Driver-Dunckley, E. D., Sabbagh, M. N., Mehta, S., Adler, C. H., and Hentz, J. G. (2016) Graph theory network function in Parkinson's disease assessed with electroencephalography. *Clinical Neurophysiology*, **127**, 2228–2236.

[41] Van Dellen, E., Douw, L., Baayen, J. C., Heimans, J. J., Ponten, S. C., Vandertop, W. P., Velis, D. N., Stam, C. J., and Reijneveld, J. C. (2009) Long-Term Effects of Temporal Lobe Epilepsy on Local Neural Networks: A Graph Theoretical Analysis of Corticography Recordings. *PLoS ONE*, **4**.

[42] van Diessen, E., Numan, T., van Dellen, E., van der Kooi, A. W., Boersma, M., Hofman, D., van Lutterveld, R., van Dijk, B. W., van Straaten, E. C., Hillebrand, A., and Stam, C. J. (2015) Opportunities and methodological challenges in EEG and MEG resting state functional brain network research. *Clinical Neurophysiology*, **126**, 1468–1481.

[43] Van Mieghem, P. and Van Langen, S. (2005) Influence of the link weight structure on the shortest path. *Physical Review E - Statistical, Nonlinear, and Soft Matter Physics*, **71**, 1–13.

[44] van Wijk, B. C. M., Stam, C. J., and Daffertshofer, A. (2010) Comparing brain networks of different size and connectivity density using graph theory. *PLoS ONE*, **5**.

[45] Varela, F., Lachaux, J. P., Rodriguez, E., and Martinerie, J. (2001) The brainweb: phase synchronization and large-scale integration. *Nature reviews. Neuroscience*, **2**, 229–239.

[46] Wu, D., Zhou, Y., Xiang, J., Tang, L., Liu, H., Huang, S., Wu, T., Chen, Q., and Wang, X. (2016) Multi-frequency analysis of brain connectivity networks in migraineurs: a magnetoencephalography study. *Journal of Headache and Pain*, **17**.

[47] Yu, M., Hillebrand, A., Tewarie, P., Meier, J., van Dijk, B., Van Mieghem, P., and Stam, C. J. (2015) Hierarchical clustering in minimum spanning trees. *Chaos*, **25**.

APPENDIX A. OVERVIEW OF 128-CHANNEL EEG LAYOUT

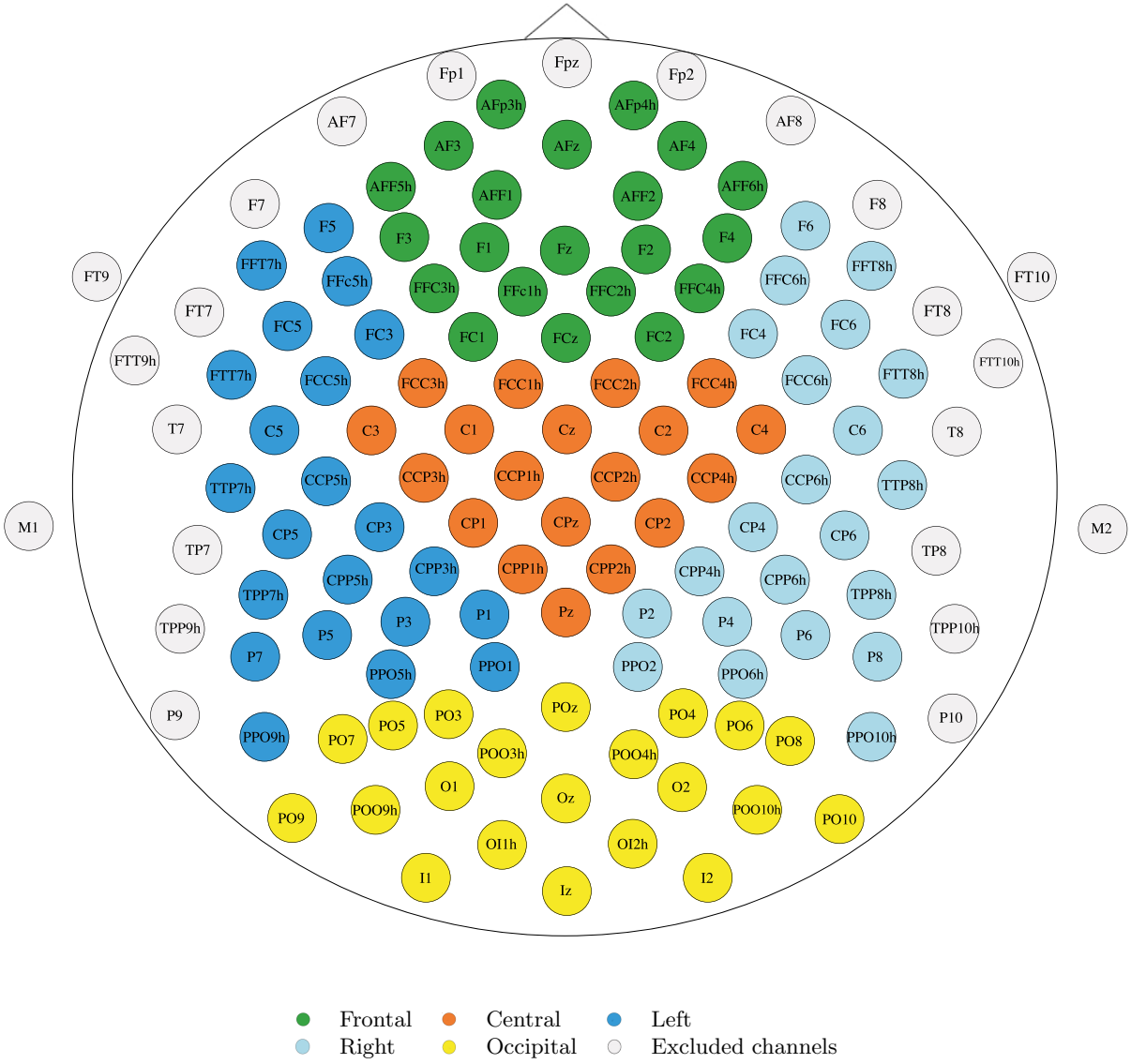

FIGURE A.1: Overview of the 128-channel EEG cap. Colors indicate which nodes belong to which cluster. Gray nodes were excluded from analyses, as scalp contact at these positions was suboptimal in most participants.

APPENDIX B. FUNCTIONAL CONNECTIVITY METHODS IN EULER NOTATION

Oscillations are described by three pieces of information: frequency, power and phase. The phase angle of a signal reveals information about the timing of frequency-band-specific activity, or the position along a sine wave of certain frequency at any given time point; that is, if the timing of two oscillations is similar, then their phase angles will have similar values. This piece of information is used as the basis for phase-based connectivity methods, like coherence and the phase-lag index (PLI). Both of these measures of synchronization are based on the *difference* in phase angles between two signals at a certain time-frequency point. Thus, in the case of frequency-band-specific data, the amount of synchronization between two signals over certain period of time (epoch) can be calculated by averaging the differences in their respective phase angles over all time points.

As phase angles are circular, the averaging of phase angle values is not straightforward. Phase angles can, however, be represented as vectors on a unit circle in the complex plane. Euler's formula (Me^ik, in which M is the magnitude and k the direction) provides a way to represent the phase information in polar space. Therefore, the phase angle difference between two signals at a certain time-frequency point can be represented by a vector on the unit plane. For all time points in frequency-band-specific data, this will result in a distribution of vectors on the unit circle.

It is the distribution of these vectors which reveals information about synchronization among the signals; that is, if the timing of the oscillations measured by the EEG electrodes is similar at each point in time in both EEG signals, then their phase angle differences will have similar values and the distribution will be clustered (see Figure B.1). On the contrary, if phase angle differences show varying values, then the distribution of their respective vectors will be more uniform.

To calculate the amount of uniformity, the vectors in polar space representing the phase angles (not the phase angles themselves) are averaged. The length of this average vector reveals how close the vectors are. In other words, the length of the average vector represents the amount of clustering of the vectors. This method forms the basis of coherence and is known as *intersite phase clustering* (ISPC). It is mathematically described by equation B.1:

$$ISPC_f = \left| n^{-1} \sum_{t=1}^{n} e^{i(\phi_{tx} - \phi_{ty})} \right| \tag{B.1}$$

in which n is the total number of time points (in this case the number of time points per epoch), the summation operator combined with n^{-1} represents the average, $\phi_{tx} - \phi_{ty}$ represent the phase angle difference of channels x and y at time point t and e^i originates from the Euler formula providing the complex polar representation of the phase angle difference at frequency f.

Spectral coherence

Spectral coherence, like ISPC, reveals the amount of clustering of the (average) vectors representing phase angle differences. The difference between both methods, is that spectral coherence is scaled by power values. In Euler notation, this gives B.2:

$$S_{xy} = \left| n^{-1} \sum_{t=1}^{n} |m_{tx}||m_{ty}| e^{i\phi_{txy}} \right| \tag{B.2}$$

in which m_x and m_y are the analytic signals of x and y respectively (Cohen, 2014).

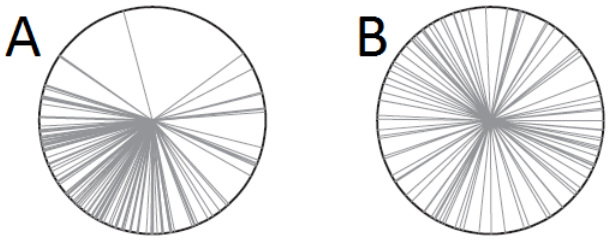

FIGURE B.1: Example of a unit circle in the complex plane representing the phase angles of many electrodes at a certain time-frequency point. A) The vectors are slightly clustered around a certain value. B) The distribution is quite uniform (Cohen, 2014).

APPENDIX C. DEGREE CORRELATION

Degree correlation indicates whether nodes tend to connect to nodes with the same or similar degree. The network is assortative if high-degree nodes connect to other high-degree nodes and similarly, low-degree nodes connect to other low-degree nodes. The network is disassortative if high-degree nodes connect with low-degree nodes, resulting in a hub-and-spoke network. More generally, degree correlation indicates if the number of links between nodes is systematically different from what is expected by chance. The probability that two nodes with degrees k and k' by chance link with each other is given by equation C.1:

$$p_{k,k'} = \frac{kk'}{2m} \tag{C.1}$$

in which m is the total number of links in the network (in this case, the MST).

The probability that a randomly chosen node will have degree k is given by p_k. However, if a randomly chosen path in the MST was followed, then the node at its end will have a degree according to a probability distribution of kp_k: high-degree nodes have more links, so the distribution is biased towards nodes of high degree. Degree correlation is about the *remaining degree*, the number of edges leaving the node other than the one that was followed. The remaining degree is one minus the total degree, giving a probability distribution of $(k+1)p_{k+1}$. Normalizing this distribution gives equation C.2:

$$q_k = \frac{(k+1)p_{k+1}}{\sum_j jp_j} \tag{C.2}$$

which is the probability that a randomly selected path in the MST has a node with degree k at its end.

The joint probability distribution of the two nodes at the ends of a path in the MST with remaining degrees k and j is given by the degree correlation matrix e_{ij}. The degree correlation matrix has the following two characteristics (equation C.3):

$$\sum_{jk} e_{jk} = 1 \qquad \sum_{j} e_{jk} = q_k \tag{C.3}$$

The amount of assortativity is given by equation C.4:

$$\langle jk \rangle - \langle j \rangle \langle k \rangle = \sum_{jk} jk(e_{jk} - q_j q_k) \tag{C.4}$$

where $\langle ... \rangle$ indicates the average over the total number of links. In order to compare the amount of assortativity among MST's, the measure is normalized by the variance $\sigma_q^2 = \sum_k k^2 q_k - [\sum_k k q_k]^2$ of the distribution q_k. Hence, the (normalized) degree correlation is (equation C.5):

$$r = \frac{1}{\sigma_q^2} \sum_{jk} jk(e_{jk} - q_j q_k) \tag{C.5}$$

r has a value between -1 and 1 and is negative for disassortative MST's and positive for assortative MST's (Newman, 2002).

APPENDIX D. MINIMUM SPANNING TREES AND CRITICAL NODES PER PARTICIPANT

COHERENCE - Migraineurs

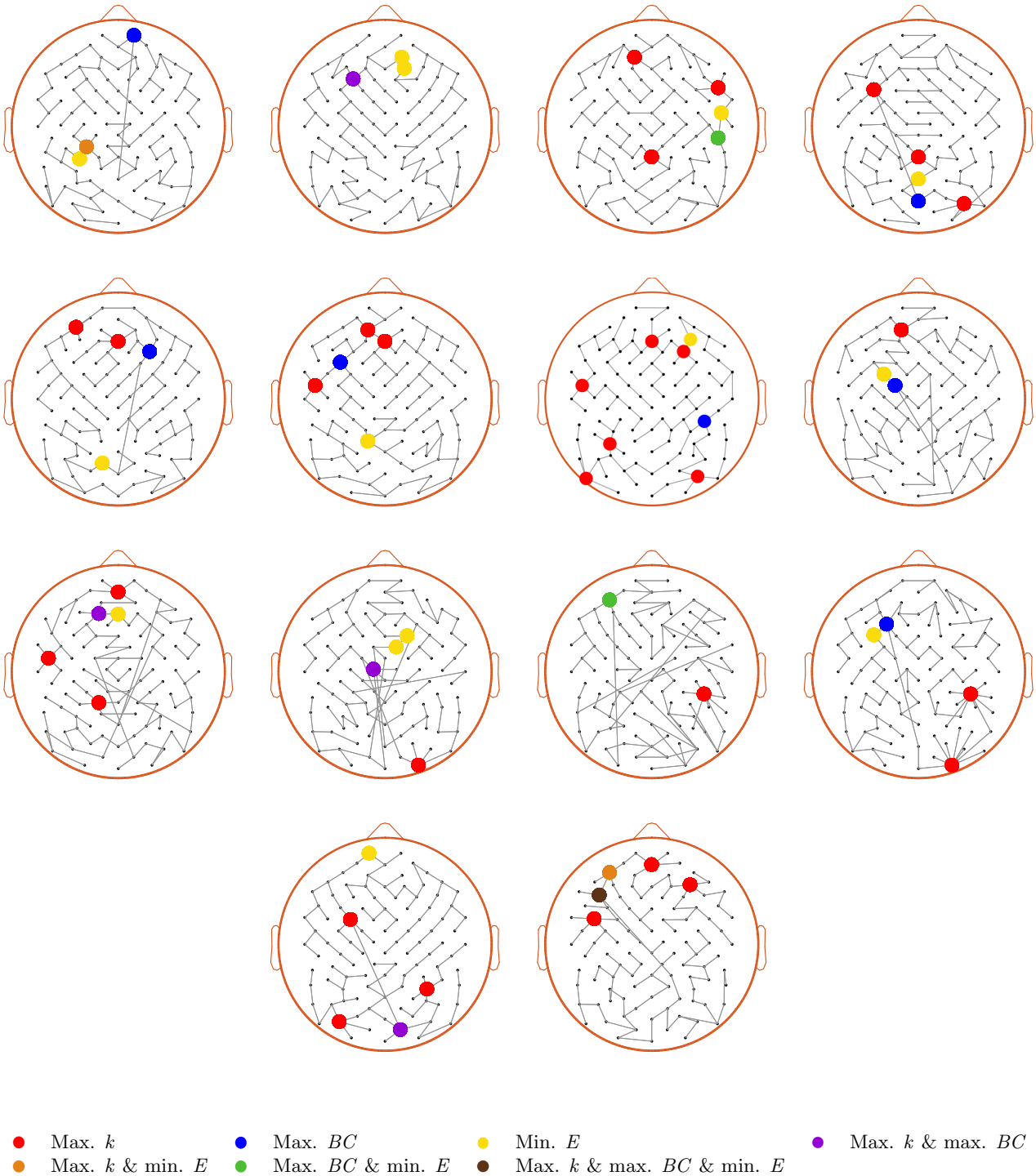

FIGURE D.1: Minimum spanning trees and critical nodes based on coherence for all participants in the migraine group. k is degree, BC is betweenness centrality and E is eccentricity.

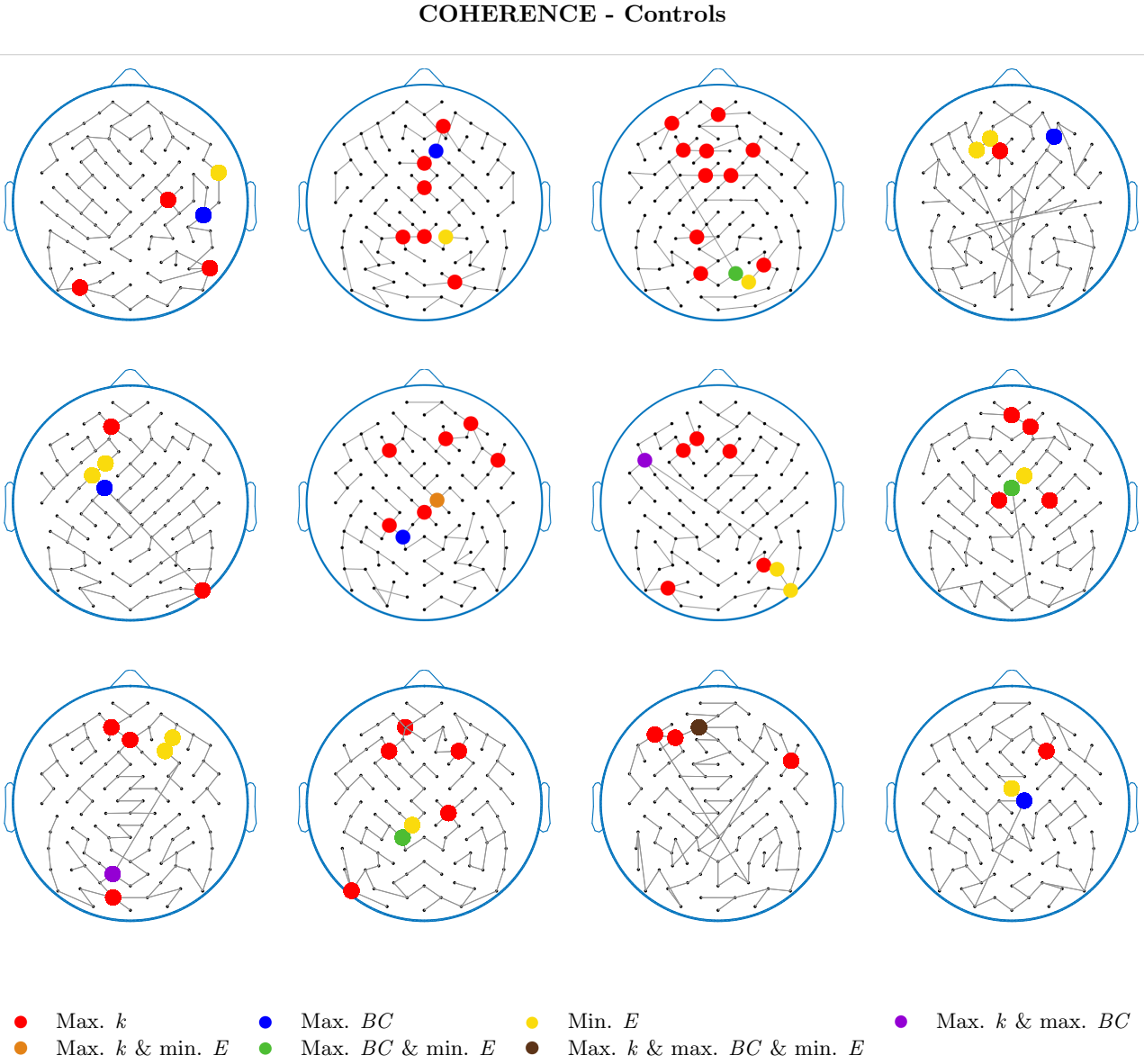

FIGURE D.2: Minimum spanning trees and critical nodes based on coherence for all participants in the control group. k is degree, BC is betweenness centrality and E is eccentricity.

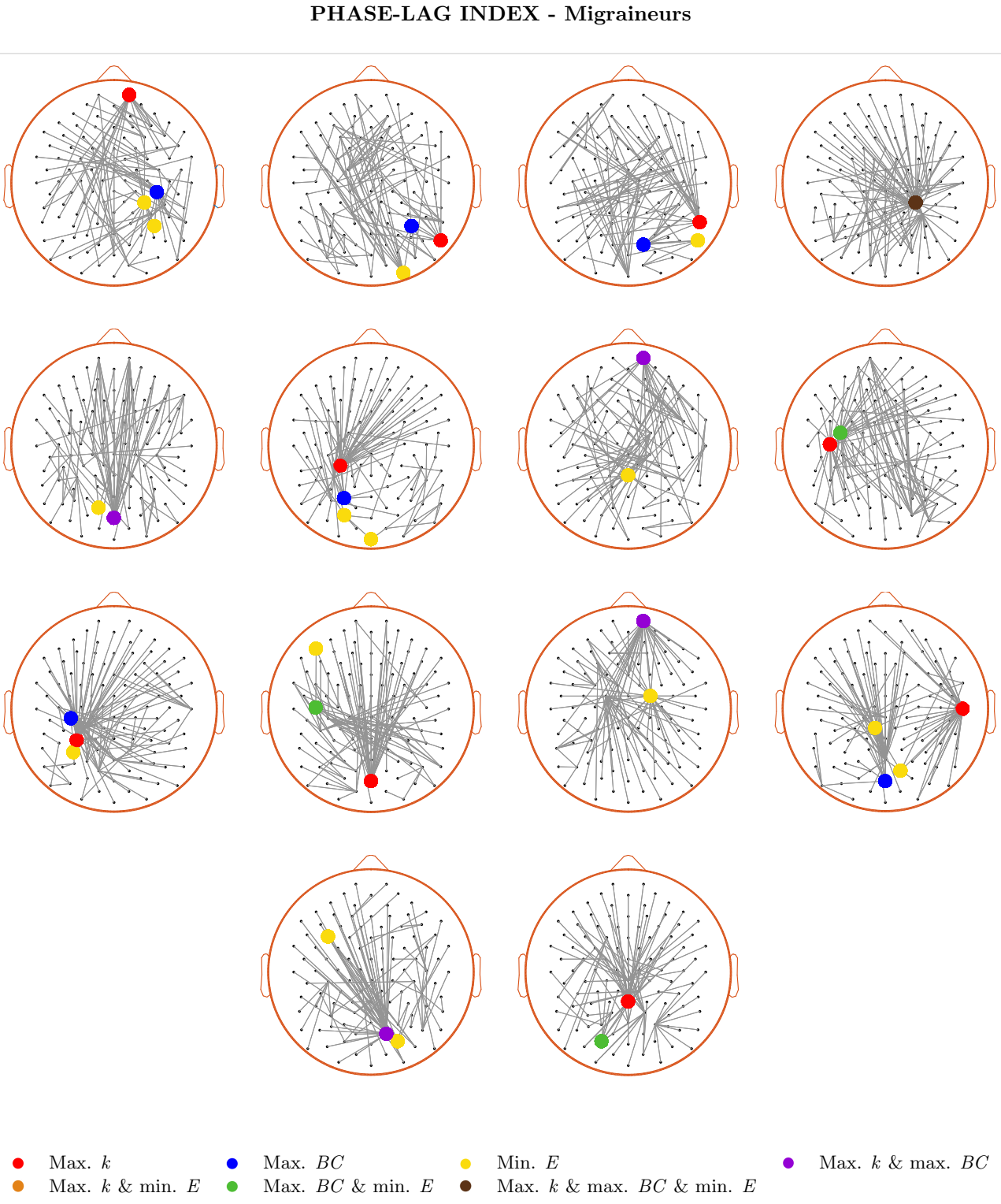

FIGURE D.3: Minimum spanning trees and critical nodes based on phase-lag index for all participants in the migraine group. k is degree, BC is betweenness centrality and E is eccentricity.

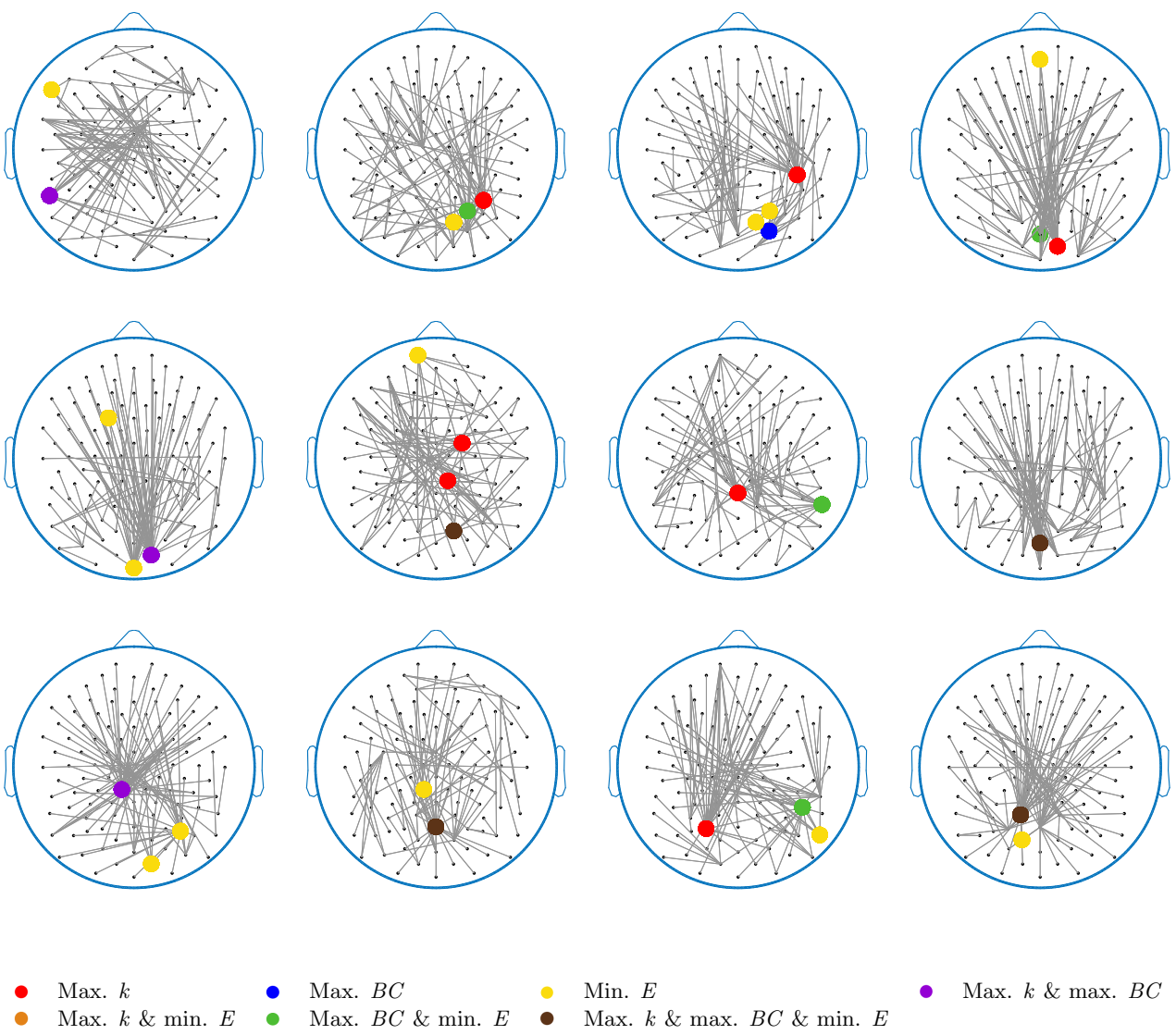

FIGURE D.4: Minimum spanning trees and critical nodes based on phase-lag index for all participants in the control group. k is degree, BC is betweenness centrality and E is eccentricity.

APPENDIX E. OVERLAP

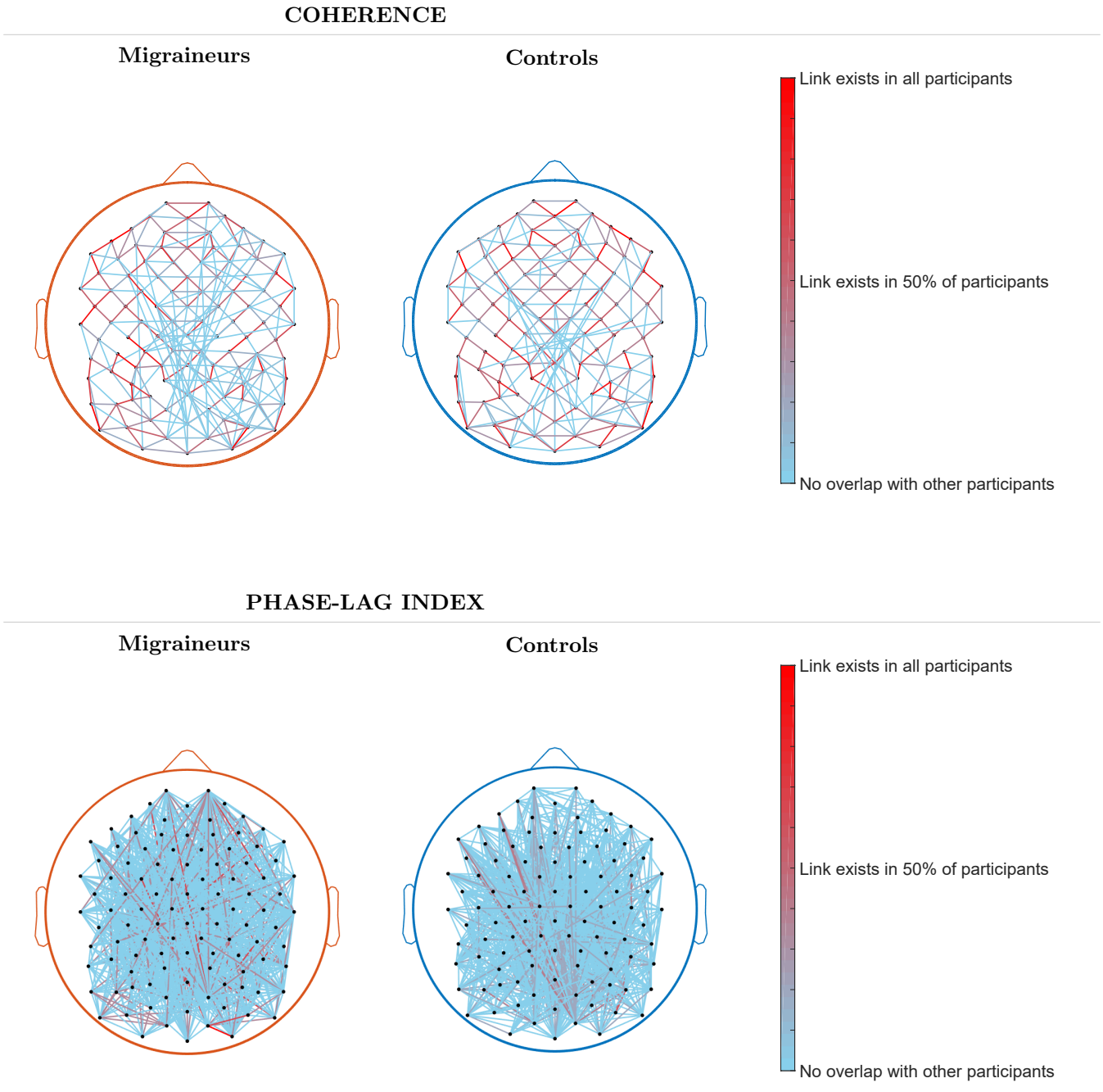

FIGURE E.1: Overlap of MST links of all participants per group. Red links indicate that the particular link exists in all participants (in that group), while light blue links appear only in individual participants.